ACS APPLIED MATERIALS & INTERFACES

RESEARCH ARTICLE

www.acsami.org

Construction of A Fluorescent Nanostructured Chitosan-Hydroxyapatite Scaffold by Nanocrystallon Induced Biomimetic Mineralization and Its Cell Biocompatibility

Guancong Wang,[†] Lin Zheng,[‡] Hongshi Zhao,[†] Junying Miao,[§] Chunhui Sun,[§] Hong Liu,[†,*] Zhen Huang,[#] Xiaoqiang Yu,[†] Jiyang Wang,[†] and Xutang Tao[†]

[†]Center of Bio & Micro/nano Functional Materials, State Key Laboratory of Crystal Materials, Shandong University, 27 Shanda Nanlu, Jinan 250100, P.R.China,

[‡]School of Medicine, Shandong University, No. 44, Wenhua Xi Road, Jinan 250012, P.R.China,

[§]Institute of Developmental Biology, College of Life Science, Shandong University, 27 Shanda Nanlu, Jinan 250100, P.R.China, and

[#]Departments of Chemistry and Biology, Georgia State University, Atlanta, Georgia 30303-3083, United States

Supporting Information

ABSTRACT: Biomaterial surfaces and their nanostructures can significantly influence cell growth and viability. Thus, manipulating surface characteristics of scaffolds can be a potential strategy to control cell functions for stem cell tissue engineering. In this study, in order to construct a hydroxyapatite (HAp) coated genipin-chitosan conjugation scaffold (HGCCS) with a well-defined HAp nanostructured surface, we have developed a simple and controllable approach that allows construction of a two-level, three-dimensional (3D) networked structure to provide sufficient calcium source and achieve desired mechanical function and mass transport (permeability and diffusion) properties. Using a nontoxic cross-linker (genipin) and a nanocrystallon induced biomimetic mineralization method, we first assembled a layer of HAp network-like nanostructure on a 3D porous chitosan-based framework. X-ray diffraction (XRD) and high resolution transmission electron microscopy (HRTEM) analysis confirm that the continuous network-like nanostructure on the channel surface of the HGCCS is composed of crystalline HAp. Compressive testing demonstrated that the strength of the HGCCS is apparently enhanced because of the strong cross-linking of genipin and the resulting reinforcement of the HAp nanonetwork. The fluorescence properties of genipin−chitosan conjugation for convenient monitoring of the 3D porous scaffold biodegradability and cell localization in the scaffold was specifically explored using confocal laser scanning microscopy (CLSM). Furthermore, through scanning electron microscope (SEM) observation and immunofluorescence measurements of F-actin, we found that the HAp network-like nanostructure on the surface of the HGCCS can influence the morphology and integrin-mediated cytoskeleton organization of rat bone marrow-derived mesenchymal stem cells (BMSCs). Based on cell proliferation assays, rat BMSCs tend to have higher viability on HGCCS in vitro. The results of this study suggest that the fluorescent two-level 3D nanostructured chitosan-HAp scaffold will be a promising scaffold for bone tissue engineering application.

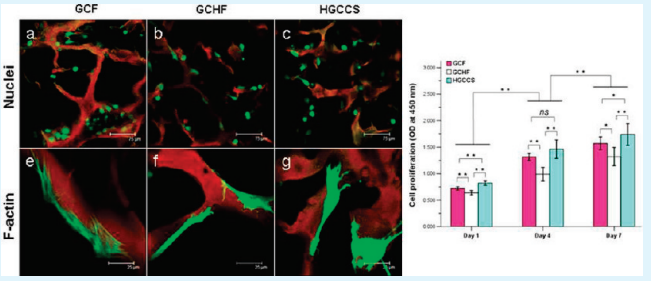

KEYWORDS: surface characteristics, nanostructure, chitosan, genipin, fluorescence, mesenchymal stem cells, bone tissue engineering

1. INTRODUCTION

Because of the limitations of the current bone substitutes, more and more patients are suffering from bone defects caused by trauma, accident, tumor and bone diseases, which especially happen to the aging population increasing rapidly in the world.[1] Bone tissue engineering has been regarded as an important strategy to repair and regenerate bone tissue through the combination of implanted cells (osteoblasts or bone marrow-derived mesenchymal stem cells), bone scaffolds and biologically active molecules (insulin-like growth factors, transforming growth factor-βs, and bone morphogenetic proteins).[2,3] An ideal scaffold, in particular, porous biodegradable polymer/hydroxyapatite (HAp) composites, should possess hierarchical porous structures to achieve the desired mechanical function and mass transport (permeability and diffusion) properties, should have a cell selective interface to enhance cell attachment and regulate cell functions, and should allow facile imaging and tracking properties.[4−6]

Although some synthetic biodegradable polymers, such as poly(glycolic acid) (PGA), poly(lactic acid) (PLA), and poly(lactic-co-glycolic acid) (PLGA), are thought as promising bone

Received: February 20, 2011
Accepted: April 14, 2011
Published: April 14, 2011

scaffold candidates, the low strength and inflammatory responses caused by release of degraded acidic products limit their applications in bone repairing.[7] Thus, derivatized biodegradable natural polymers, including polysaccharides (alginate, chitin/chitosan, and hyaluronic acid derivatives) and proteins (collagen, gelatin, and silk), have become the most important and promising polymers for preparation of bone tissue scaffold. Collagen, one of the most important natural biodegradable polymers and the main organic component of bone tissue and extracellular matrix (ECM), has great advantage as a supporting scaffold for bone tissue engineering.[8,9] However, the complicated extraction process, high cost, and low strength are the major obstacles for broad medical applications of collagen-based bone tissue scaffold.

As another important biodegradable natural polymers, chitosan [poly-1,4-D-glucosamine, $(C_6H_{11}O_4N)n$)], a partially deacetylated derivative from chitin, is structurally similar to glycosaminoglycan (GAG) and is a mimic of the natural extracellular matrix (ECM). It has been studied in various biomedical applications including tissue engineering for skin, bone, blood vessels, and nerves because of its ready availability, biocompatibility, biodegradability, osteoconductivity, cationic nature, flexible adhesiveness, and antibacterial and wound-healing activity.[10,11] Presently, the fabrication techniques for porous HAp/chitosan composite bone scaffolds are based on either mixing or in situ coprecipitation methods.[12,13] The mixing method involves blending synthetic HAp nanoparticles into a chitosan solution, followed by cross-linking and lyophilization. The in situ coprecipitation method involves stepwise dropping of Ca^{2+} and $PO4^{3-}$ solutions into a chitosan solution. In addition, a few different methods have been reported, such as in situ hybridization by ionic diffusion processes and mineralization via a double diffusion technique.[14,15] Though the mixing and in situ coprecipitation approaches are simple processes with low cost, it is difficult to control the surface chemistry and geometry within a large and complex structure. In addition, these methods for chitosan/HAp scaffold preparation normally use glutaraldehyde (GTA) as a cross-linker, a substance that is toxic when it is released in the host during the biodegradation process.[16]

To develop ideal bonelike composites with enhanced mechanical properties and improved bioactivity, biomimetic mineralization has become an effective strategy to assemble bonelike apatite that is close to natural bone with low crystallinity and nanoscale size.[17−19] However, it is difficult to achieve the controlled nucleation and growth of HAp nanocrystals on a chitosan-based framework because of its smooth surface.[20,21] Though it has been reported that a chitosan/nano-HAp composite scaffold can be formed via biomimetic mineralization using simulated body fluid (SBF),[22,23] the HAp layer obtained has irregular morphology. Thus, it is critical to control and attain desirable bioactive mineral surface structures within a chitosan-based framework through a nontoxic and controllable preparation method, and it is still a great challenge for bone tissue engineering.

In this work, we report a strategy to meet these critical needs for the bone tissue scaffold. First, genipin (a nontoxic natural cross-linker), an aglycone of geniposide extracted from gardenia fruit,[24] is used to prepare the chitosan framework. The cross-linker not only enhances the scaffold strength but also provides intrinsic fluorescence to the composite scaffold. Previous studies have investigated the fluorogenic characteristics of the chitosan−genipin membrane and microcapsule,[25,26] and have used genipin as a cross-linker to fabricate a chitosan based scaffold.[27,28] Rather than be concerned with other bone tissue scaffolds, we further explore this fluorescence property that provides effective ways for imaging the scaffold-cell interface, tracing adhesion, following migration and cell proliferation, and for investigating the scaffold degradation process with a confocal laser scanning microscope (CLSM). Second, a nanocrystallon induced biomimetic mineralization method was designed to achieve control of the assembly and morphology of HAp nanostructures on the channel surface of the chitosan framework through an in vitro biomimetic mineralization process in SBF.[29] The HAp-coated genipin-chitosan conjugation scaffold (HGCCS) possesses a two-level, three-dimenional (3D) porous structure to provide sufficient calcium source and achieve desired mechanical function and mass transport properties.

To characterize biocompatibility of bone tissue scaffolds, MC3T3-E1 mouse preosteoblast cells have been extensively used.[19,30] Bone marrow-derived mesenchymal stem cells (BMSCs) isolated from bone marrow have attracted particular attention in bone tissue engineering because of their self-renewal and high differentiation potentials.[31,32] Recent studies have indicated that the surface characteristics of biomaterials, such as chemical composition, roughness, and topography, especially nanotopography, can significantly influence cell growth and cell differentiation[33−35] that may be attributed to mechanical factors through cytoskeletal tension/RhoA/ROCK.[36,37] Thus, manipulating the surface characteristics of bone tissue scaffolds is an effective strategy to control cellular behavior and differentiation for stem cell tissue engineering and bone regeneration. Literature reports indicate that MC 3T3 cells adhere preferentially to and proliferate in regions with flakelike and highly nanotextured calcium phosphate that is mineralized on the poly(lactic-co-glycolic acid) (PLGA) nanofiber-based scaffold.[19] We report here further observation of the impact of the HAp surface nanostructure obtained by biomimetic mineralization on the adhesion, morphology, proliferation, and cytoskeletal organization of rat BMSCs.

2. EXPERIMENTAL SECTION

2.1. Materials. Chitosan ($M_n \approx$ 20 000 and >90% deacetylated) was obtained from Hai Debei Co. Ltd. (Jinan, China). $Ca(NO_3)_2 \cdot 4H_2O$, $(NH_4)_2 \cdot HPO_4$) and all the inorganic salts for SBF were of analytical grade and purchased from Sinopharm Chemical Reagent Co. Ltd. (Shanghai, China). Genpin was purchased from Hu Yun Co. Ltd. (Shanghai, China). Dulbecco's Modified Eagles Medium (DMEM, Low Glucose), fetal bovine serum (FBS), and penicillin-streptomycin were procured from Gibico (USA).

2.2. Synthesis of Nano-HAp. HAp nanorods were synthesized through a hydrothermal method by using calcium nitrate tetrahydrate ($Ca(NO_3)_2 \cdot 4H_2O$) and diammonium hydrogen phosphate ($(NH_4)_2 \cdot HPO_4$)) as reactants.[38] Stock solutions were prepared by respectively dissolving 10 g $Ca(NO_3)_2 \cdot 4H_2O$ and 3.35 g $(NH_4) \cdot 2HPO_4$ in 70.0 and 80.0 mL of distilled water, arriving at a pH of 11.0 and a pH of 10.0 using ammonia. Subsequently, the stock solutions were mixed to yield suspensions with Ca/P molar ratios of 1.67 by the dropwise addition of the $Ca(NO_3)_2$ solution to the $(NH_4)_2HPO_4$ solution with vigorous stirring. The precipitate was then transferred to a 25 mL Teflon hydrothermal reactor. The reaction was initiated by placing the unit in a laboratory oven for 20 h at a temperature of 200 °C. The product powder was washed twice with distilled water and once with ethanol. Finally, the HAp powder obtained by filtration and drying at 60 °C was characterized by transmission electron microscopy (TEM) and X-ray diffraction (XRD) (see Figure S1 in the Supporting Information).

2.3. Preparation of Genipin-Cross-Linked Chitosan Framework (GCF). GCF was prepared in two steps: cross-linking and

freeze-drying. Briefly, 1 g of chitosan was dissolved overnight in 20 mL of acetic acid (2 vol.%) to obtain a 2% chitosan solution, then 100 μL ethanol containing 0.005 g genipin with a chitosan/genipin mass ratio = 200:1 was added to complete the cross-linking reaction after 12 h at room temperature. Subsequently, the genipin-cross-linked chitosan gel was frozen by being held at −80 °C for 5 h and then lyophilized by holding at −50 °C for 48 h to obtain GCF. The resulting framework was neutralized using a 0.1 M sodium hydroxide solution.

2.4. Preparation of Genipin-Cross-Linked Chitosan/Nano-HAp Composite Framework (GCHF). The preparation of GCHF was similar to that of the genipin-cross-linked chitosan framework, as described above. To obtain a genipin-cross-linked chitosan/nano-HAp composite framework, 0.5 g of nano-HAp powder (mass ratio of chitosan to nano-HAp of 2:1) was blended into a chitosan solution with vigorous stirring for 24 h, before being cross-linked by genipin and lyophilized. The resulting framework was then neutralized using a 0.1 M sodium hydroxide solution.

2.5. Biomimetic Mineralization for Construction of HAp-Coated Genipin−Chitosan Conjugation Scaffold (HGCCS). Simulated body fluid (SBF) was prepared in accordance with Kokubo's method.[30] The ion concentrations (mM) are as follows: Na^+ (142 mM), K^+ (5 mM), Mg^{2+} (1.5 mM), Ca^{2+} (2.5 mM), Cl^- (120 mM), HCO_3^- (27 mM), HPO_4^{2-} (2.27 mM), SO_4^{2-} (0.5 mM). NaCl (8.035 g), $NaHCO_3$ (0.355 g), KCl (0.225 g), $K_2HPO_4 \cdot 3H_2O$ (0.231 g), $MgCl_2 \cdot 6H_2O$ (0.311 g), 1 M HCl (38 mL), $CaCl_2 \cdot 2H_2O$ (0.3675 g), $NaSO_4 \cdot 10H_2O$ (0.071 g), and $NH_2C(CH_2OH)_3$ (*Tris*, 6.118 g).

GCF and GCHF were cut into discs of 15 mm in diameter and 2 mm thickness, then soaked in 1 L of SBF in an incubation box at 37 °C for 2, 4, and 8 days to obtain HGCCS. Finally, the HGCCS was washed with deionized H_2O, frozen at −80 °C, and lyophilized at −50 °C for 6 h. In addition, a cylinder-shaped sample of HGCCS of 10 mm in length and 15 mm in diameter was prepared by the same method.

2.6. SEM Observation. A SEM (S-4800, Hitachi, Japan) was used to characterize the morphology of GCF, GCHF and the biomimetic mineralization of HAp growth on the channel wall of the framework at an accelerating voltage of 10 kV.

2.7. X-ray Diffraction (XRD) and High-Resolution Transmission Electron Microscopy (HRTEM) Analysis. XRD data were recorded on a Japan Burkert D8/advance X-ray diffractometer system with graphite monochromatized Cu Kα irradiation (λ = 0.15418 nm), with a scan step size of 2θ = 0.02°, and a dwell time of 2 s/step, over a 2θ range of 10−70°. HRTEM observations were carried out with a JEM-2100 (Japan) instrument operated in the transmission mode at 200 kV. The sample was prepared following the protocols referred to as Olszta's method.[39]

2.8. Mechanical Testing. Compressive testing is commonly used to evaluate the mechanical properties of bone scaffolds.[40,41] Prior to the test, pure chitosan without cross-linkage (denoted as PC), GCF, GCHF and HGCCS were cut into cylindrical samples with a 2:3 aspect ratio (10 mm in length and 15 mm in diameter). Compressive testing was performed on a computer-controlled WDW-1 universal material testing machine with a cross head speed of 5 mm/min maintained until failure. The compressive elastic modulus was calculated from the initial slope of the stress−strain curve.[42,12] The value reported is the average of measurements on at least five specimens (n = 5).

2.9. CLSM Observation for Genipin-Cross-Linked Chitosan Framework (GCF) before and after Degradation Process. CLSM (Leica, Germany) was used to study the fluorescence and the change in the 3-dimensional microstructure of porous GCF. Enzymatic degradation was performed by immersing the materials in 5 mg/mL lysozyme in a sterile phosphate buffer saline solution (PBS, pH 7.4) at 37 °C for 48 h. A series of slices was obtained from a tomoscan with 10 μm thick sections along the z-axis of the GCF. Then, the confocal image of 3D porous GCF to a depth of 100 μm was obtained through 3D image reconstruction. The excitation wavelength was 488 nm.

2.10. Rat BMSCs Isolation and Culture. Rat BMSCs were isolated from femurs and tibias of 30 day old neonatal male Wista rats procured from the Animal Experimental Center of Shangdong University (Jinan, China) with a modified method originally described by Pittenger et al.[43] The cells were cultured in vitro using DMEM (Low Glucose) supplemented with 1% penicillin-streptomycin at 37 °C, 5% CO_2 and 95% humidity. Rat BMSCs were phenotypically characterized by the method published by Wang et al.[44] Cells were seeded on scaffolds after 3 passes (2 days for pass 1).

2.11. Cell Culture on Disklike Samples. GCF, GCHF and HGCCS were cut into disk-like samples with 15 mm diameter and 2 mm thickness. Subsequently, all the samples were sterilized by immersing them in 75% ethanol for 30 min, exposing them to UV radiation for 30 min on each side, and then washing each three times in a sterile phosphate saline buffer solution (PBS, pH 7.4). These samples were placed in 24-well plates and seeded with 500 μL of cell suspension containing 2.0×10^5 rat BMSCs on each disk for 2 h. Another 500 μL of fresh culture medium was then added to each disk. The culture was maintained up to 7 days in an incubator at 37 °C, 5% CO_2, and 95% humidity. The culture media were changed every 3 days.

2.12. Evaluation of Cell Adhesion and Morphology. After 3 days of culturing, the cell-seeded discs (n = 2) were removed from the culture and gently washed with PBS. The cells on the discs were immobilized with 2.5% glutaraldehyde in PBS for 30 min at 4 °C. After removing the fixative, the disks were subsequently gently washed in PBS and distilled water. These samples were subjected to sequential dehydration for 10 min each with an ethanol series (30, 50, 70, 85, 90, 95, and 100%). Further, samples were allowed to dry for a day, coated with platinum for 40 s, and examined with a SEM for cell adhesion and morphology. All samples were observed at a 3 kV accelerating voltage.

2.13. Cell Proliferation. A cell count kit-8 (CCK-8, Dojindo, Japan) was employed in the experiment to quantitatively evaluate cell viability on various scaffolds after cultivation for 1, 4, and 7 days. Briefly, for each sample (or scaffold), the original medium was replaced by 500 μL serum-free DMEM medium containing 50 μL CCK-8 solution, followed by incubation at 37 °C for 3 h. After the formed formazan solution (100 μL) was taken from each sample and transferred to one well of a 96-well plate, the absorbance at 450 nm was determined using a microplate reader (Bio-Rad, USA). Six parallel replicates (n = 6) for each sample were used to assess cell proliferation.

2.14. Assessment of Cell Localization and Cytoskeleton Organization. After 3 days of culturing, the localization and cytoskeleton organization of the adherent cells on samples stained with nucleic acid dye, acridine orange (AO) (Invitrogen) and Alexa Fluor 488 phalloidin (Invitrogen), respectively, were examined using CLSM. Briefly, for staining the nuclei, the cell-loaded samples removed from the culture media were fixed with 4% paraformaldehyde for 1 min, and then stained in 0.01% acridine orange (AO) solution for 1 min. For immunofluorescence measurements of F-actin, the cell-loaded samples were fixed with 3.7% formaldehyde solution for 10 min, then extracted with 0.1% Triton X-100 (Sigma) for 5 min and blocked with PBS containing 1% bovine serum albumin (BSA) (Sigma) for 30 min. The samples were then stained with phalloidin conjugated to Alexa Fluor 488 and examined at excitation wavelengths of 488 and 633 nm.

2.15. Statistical Analysis. The statistical analysis of all the experimental data was performed using SPSS version 11.0 (SPSS Inc., Chicago, Illinois). Data were reported as the mean ± standard deviation. Statistical comparisons were performed by ANOVA for multiple comparisons, and statistical significance was accepted at $p < 0.05$.

3. RESULTS AND DISCUSSION

3.1. SEM Observation of Construction of the Composite Scaffold. From Figure 1a, we can see that genipin-cross-linked-chitosan framework (GCF) is a macroporous structure with 3D

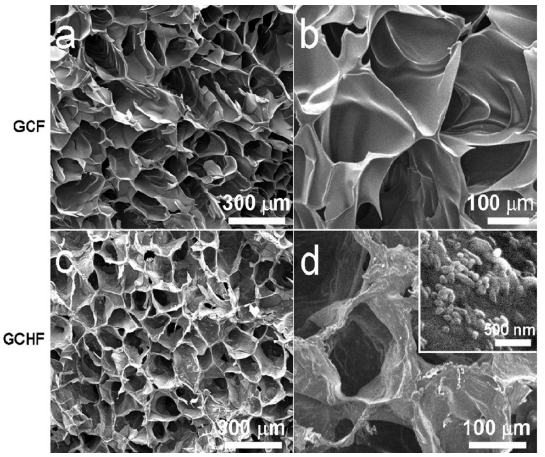

Figure 1. SEM images of (a, b) genipin-cross-linked chitosan framework (GCF) and (c, d) genipin-cross-linked chitosan/nano-HAp composite framework (GCHF).

interconnected channels. The average diameter of a channel is about 150−200 μm, and its wall thickness is about 5 μm, a value that is favorable for cell immigration and mass transport (Figure 1b). Figure 1c shows that the genipin-cross-linked-chitosan/nano-HAp composite framework (GCHF) retains the 3D interconnected microstructure of the chitosan framework with a pore size of 150−200 μm. However, instead of the clean smooth channel surface of the GCF, there is a large number of HAp nanorods serving as nanocrystallons that are laid on the channel surface of the GCHF (Figure 1d), which provide sufficient seeds for the growth of HAp nanocrystals and for nanostructure assembly during the biomimetic mineralization process. In addition, the GCHF channel wall becomes a little thicker than that of GCF due to the incorporation of nano-HAp (Figure 1b,d).

Figure 2 shows SEM images of samples at different stages of preparation for HGCCS. The GCF was used for attempting to construct HGCCS by coating a layer of nano-HAp on its channel surface through a biomimetic mineralization method using SBF. However, mineralization on the channel surface of GCF is difficult to realize. After immersing in SBF even for 8 days, only a few bulges are found on the channel surface (Figure 2a, b).

Therefore, to achieve a well-structured HAp nanostructure on the channel surface of chitosan framework, a nanocrystallon induced biomimetic mineralization method was employed. The idea of this method is to pack HAp nanorods of ∼20 nm in diameter and ∼150 nm in length as nanocrystallons on the chitosan framework (corresponding to GCHF), and then to grow the HAp nanocrystals on the top of the nanocrystallons during the mineralization process. This method is imitated from a top-seeding growth process of bulk crystals, and hence is defined as nanocrystallon-induced biomimetic mineralization method.

After mineralization of GCHF for 2 days in SBF, some petal-like nanostructures connected to the ends of the HAp nanocrystals were found on the channel surface of GCHF (Figure 2c and d). After mineralization for 4 days in SBF, some pieces of self-assembled nanonetworks appeared on the channel surface of GCHF (Figure 2e, f); the network building blocks are petal-like nanostructures similar to those in the 2-day mineralization sample. After mineralization for 8 days in SBF, GCHF retains 3D porous structure with interconnected channel with the pore size of ∼150 μm and the channel wall becomes thicker (Figure 2g). Importantly, the channel surface of GCHF including the internal pore structure (designated by the black arrow in Figure 2h) is completely covered with a uniform and continuous nanonetwork with a ∼150 nm pore diameter (Figure 2g, h).

Therefore, a two-level, 3D interconnected network scaffold (HAp-coated genipin-chitosan conjugation scaffold, HGCCS) was realized. The first level of the network is the chitosan/nano-HAp 3D interconnected macroporous framework (Figure 2g); the second level of the network is self-assembled by the mineral nanonetwork (Figure 2h). Mass measurements show that the mass percentage of the HAp nanonetwork layer is about 29%. The above results indicate that nanocrystalline HAp seeds play a determining role in the construction of the calcium-phosphate nanonetwork on the channel surface of GCHF.

When the assembly of a layer of a biomimetic apatite nanostructure throughout a 3D porous bone tissue engineering scaffold, such as biodegradable polymer/HAp composites is realized, it represents a practical method of controlling the surface chemistry and geometry within a large and complex structure. To the best of our knowledge, this work represents the first successfully assembled and well-defined layer of a HAp networklike nanostructure on a 3D chitosan-based framework.

3.2. Structural Characterization. To characterize the phase structure of the nanonetwork on the channel surface of HGCCS, XRD analysis was carried out. Figure 3 shows the XRD pattern of all the samples. A very broad peak in the XRD pattern of GCF centered at about 22° is attributed to genipin-cross-linked chitosan (Figure 3a). Figure 3b shows a similar peak to that in Figure 3a, indicating that there is no crystalline calcium phosphate or apatite formed on GCF after mineralization in SBF for 8 days. The bulges on the channel surface of GCF thus represent an amorphous phase. The result further confirms that it is difficult to realize mineralization on the channel surface of GCF. Figure 3c shows the XRD pattern of GCHF. All the peaks of this pattern can be indexed to the hexagonal HAp crystal of space group P63/m ($a = b = 9.418$ Å, $c = 6.884$ Å) (PDF Card No.09−432), corresponding to the peaks of as-synthesized HAp nanocrystals (Figure 3e). For the HGCCS sample (after biomimetic mineralization in SBF for 8 days), the positions of all the peaks in the XRD pattern are the same as those in the GCHF pattern, but most of them appear sharper and stronger (Figure 3d).

In order to further confirm the phase structure of the nanonetwork, HRTEM observation on the petal-like nanocrystals was performed with a JEM-2100 (Japan) TEM. The HRTEM sample was prepared by separating the petal-like HAp nanoflakes from HGCCS following Olszta's method.[39] The HRTEM image (Figure 4a) shows hydroxyapatite nanocrystal rods inducing mineralization and nanopetals growing on the channel surface of GCHF (Figure 4a). The crystalline lattice image (Figure 4b) of the petal-like crystals reveals a plane spacing of 3.43 Å, corresponding to the apatite (002) lattice plane, which further confirms that the continuous nanonetwork on the channel surface is composed of crystalline HAp. In addition, the structural development of the composite was also confirmed by Fourier transform infrared spectroscopy (FTIR) (see Figure S2 in the Supporting Information).

In short, this result implies that the only mineral phase in HGCCS is HAp, and no other crystalline phase, such as calcium carbonate or other calcium phosphate compounds form during the entire mineralization process.

3.3. Mechanical Properties. Generally, the compressive elastic modulus (EM) is used to evaluate the mechanical properties of bone scaffolds.[40,41] Figure 5 shows the EM of different

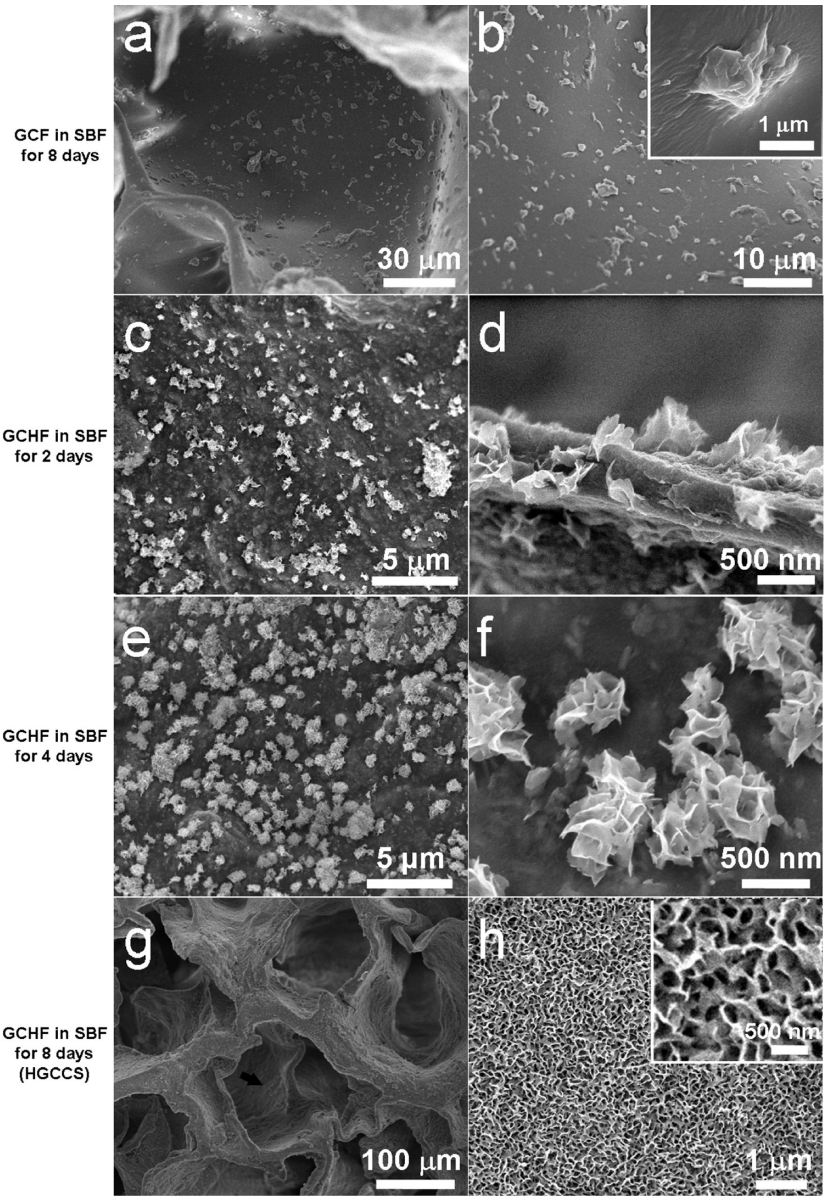

Figure 2. SEM images of samples at different stages of preparation for HAp coated genipin-chitosan conjugation scaffold (HGCCS). (a, b) Genipin-cross-linked chitosan framework (GCF) mineralized in SBF for 8 days, genipin-cross-linked chitosan/nano-HAp composite framework (GCHF) mineralized in SBF for (c, d) 2, (e, f) 4, and (g, h) 8 days (HGCCS).

groups of samples: pure chitosan without cross-linkage, GCF, GCHF, and HGCCS. The EM of PC is only 1.84 ± 0.65 MPa, and that of GCF is 30.68 ± 2.35 MPa, which is about 10 times higher than 2.9 ± 0.4 MPa, the previously reported EM value of a chitosan scaffold.[45] This result implies that the nontoxic cross-linker, genipin, has a strong cross-linking ability and apparently improves the strength of the framework. The EM of GCHF is 41.88 ± 3.13 MPa, which is higher than that of GCF, indicating a reinforcement of the HAp nanorods for the framework. The reinforcement effect of HAp nanorods is caused by their rodlike morphology and the specific binding force produced by the nanocrystal $-OH^-$ groups and the $-NH_2$ groups at the chitosan chains,[12] in keeping with the well-known whisker-reinforcement mechanism.[46]

After biomimetic mineralization in SBF, the EM of the HGCCS obtained increases to 50.49 ± 2.23 MPa, which is about 17% higher than that of GCHF without mineralization. This result indicates that the HAp network-like nanostructures formed on the channel walls of GCHF through mineralization exhibit a strong support and reinforcement effect that resists compression. Based on the strong cross-linking ability and effective reinforcement of the HAp nanonetwork self-assembled on the channel wall of porous GCHF, the strength of the HGCCS obtained in this way exhibits experiences an apparent enhancement.

3.4. Intrinsic Fluorescent Property of GCF and the Change of Microstructure before and after Degradation. From Figure 6, we observe the pore size and microstructure of the interconnected channels in 3D porous GCF by CLSM at excitation wavelength of 488 nm before degradation with a depth to a depth 100 μm from the 3D reconstructed image. More importantly, compared to the SEM observations, the depth dependent images of the laser confocal fluorescence measurement from the 3D

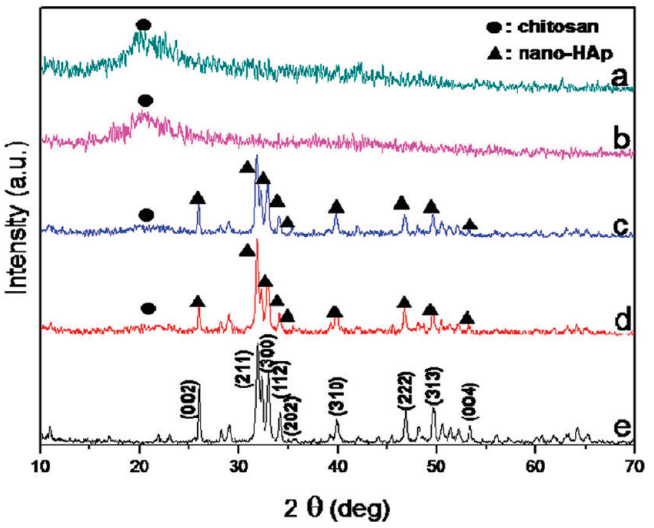

Figure 3. X-ray diffraction patterns of (a) genipin-cross-linked chitosan framework (GCF), (b) GCF biomimetic mineralized in SBF for 8 days, (c) genipin-cross-linked chitosan/nano-HAp composite framework (GCHF), (d) HAp coated genipin-chitosan conjugation scaffold (HGCCS), and (e) HAp nanorods synthesized by a hydrothermal method.

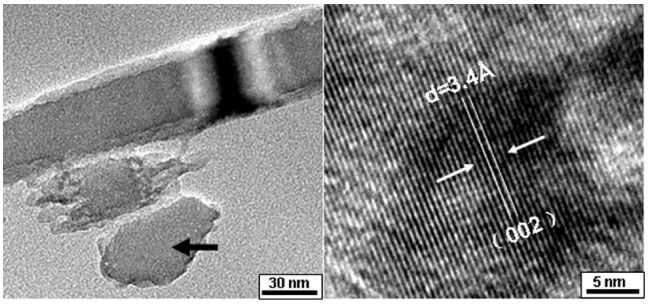

Figure 4. HRTEM images of petal-like nanocrstals eroded from HGCCS. (a) HAp petals formed by biomimetic mineralization in SBF. (b) Higher-magnification view of the petals indicated by the black arrow in a.

reconstruction demonstrate a true 3D scaffold with interconnected channels. In addition, observation of a series of slices (randomly selected section numbers 1, 6, and 10) from a tomoscan with 10 μm thick sections along the z-axis provides more information on the 3D microstructure of the scaffold, such as cross-section display homogeneity and interconnectivity of the GCF. The formation of these images can be attributed to the intrinsic fluorescence of genipin-cross-linked chitosan. In GCHF and HGCCS the same fluorescence is also displayed in subsequent CLMS observation (Figure 9 and Figure S3 in the Supporting Information).

In addition, we observe by CLSM the change in the GCF microstructure before and after enzyme degradation by fluorescence. Compared to the interconnected channels of 3D porous GCF before degradation, it appears that the channels have collapsed, and the microstructure has become irregular with no uniform pore size after the enzymatic degradation process in a 5 mg/mL lysozyme solution at 37 °C for 48 h.

Recently, fluorescent biomaterials have attracted much attention, because of the great demand for imaging and tracking of

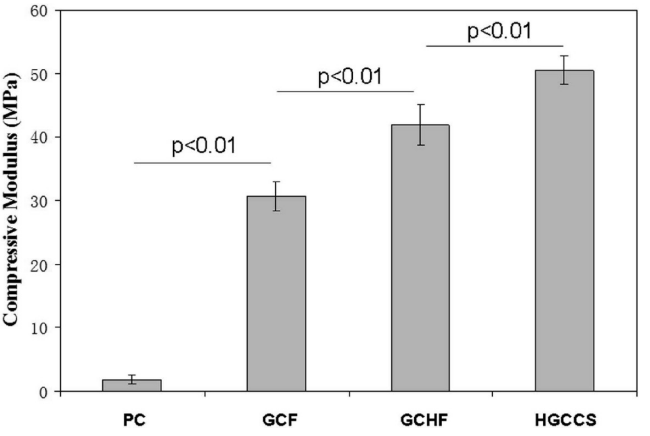

Figure 5. Compressive elastic modulus of noncross-linked chitosan (PC), genipin-cross-linked chitosan framework (GCF), genipin-cross-linked chitosan/nano-HAp composite framework (GCHF), and HAp coated genipin-chitosan conjugation scaffold (HGCCS). Error bars indicate standard deviation (n = 5).

biomaterials during medical research or treatment. Some approaches to the preparation of chitosan-based fluorescent materials are suggested. However, most of them are related to labeling with fluorescent particles or molecules, such as fluorescein isothiocyanate (FITC), which results in a more complicated process or involves toxic chemicals. At the same time, the fluorogenic characteristics of the chitosan−genipin membrane and microcapsule have been observed by some researchers. Previous studies reported that the large conjugated system, possibly the $\pi-\pi^*$ conjugation formed by the chitosan and genipin reaction, is the likely photophysical origin of this emission.[25] It was also found that reaction conditions, including pH, temperature and time, can affect the fluorescence intensity of the product.[26] We further explore the novel fluorescence properties that suggest a promising application for 3D scaffold imaging and tracking using CLSM without toxic additions, and in situ observation of the degradation process in vivo or in vitro.

3.5. Cell Adhesion and Morphology. As shown in Figure 7, the morphology of rat BMSCs exhibits a notable change after culturing for 3 days on the channel surface of GCF, GCHF and HGCCS. Rat BMSCs on the channel surface of GCF adhere, spread and appear confluent (Figure 7a,b). In addition, the spindle morphology looks like the typical BMSCs phenotype, which is different from previous results reported by RDK Misra on MC 3T3-E1 cultured on a chitosan scaffold.[12] On the channel surface of GCHF, the cells become thicker and exhibit a fibroblastic morphology with extensive cellular processes (Figure 7c,d). As shown in Figure 7d from lateral observation, BMSCs display weaker adhesion to the surface of GCHF. The following proliferation assay further indicates a lower viability compared to GCHF and HGCCS.

With regard to two-level, 3D HGCCS, the cells are flat and broad with very large area, and tightly adhere to the channel surface of the scaffold (Figure 7e). Moreover, a much more pronounced protrusions of pseudopodia contact with the surface network-like HAp nanostructures (Figure 7f). Similar behavior was observed for bovine aortic endothelial cells.[47]

The above experiments prove that rat BMSCs on HGCSSC present much better attachment. The results also indicate that the morphology of rat BMSCs can be affected by the surface morphology and the channel surface structure of the scaffolds. As is

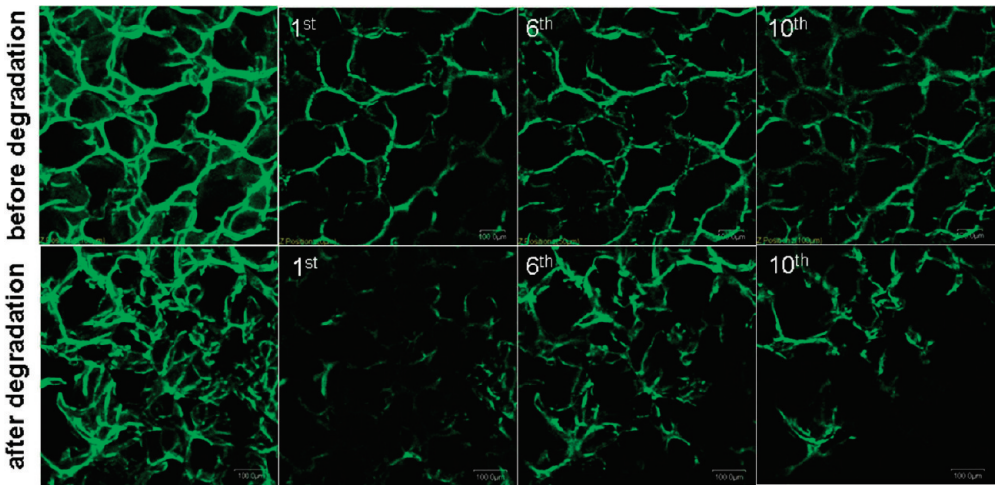

Figure 6. Confocal laser scanning micrographs of 3-dimensional porous genipin-cross-linked chitosan framework (GCF) (before and after degradation) to a depth of 100 μm through 3-dimensional image reconstruction and a series of tomoscan slices with 10 μm thick sections along the *z*-axis. Randomly selected section numbers 1, 6, and 10 are presented. The excitation wavelength is 488 nm.

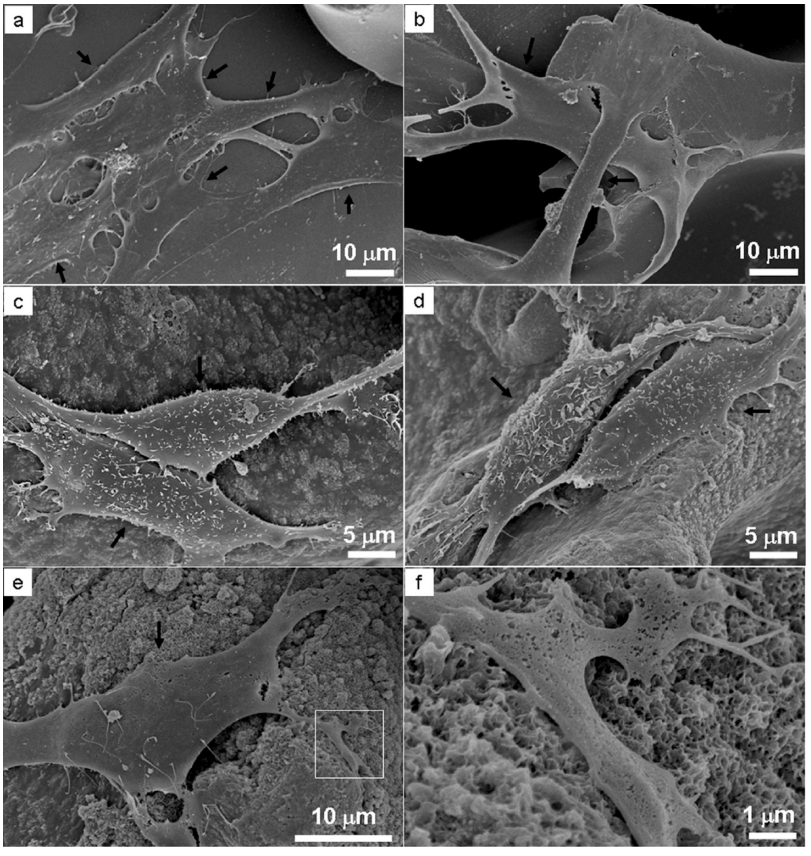

Figure 7. SEM images of rat BMSCs on genipin-cross-linked chitosan framework (GCF) (a, b), genipin-cross-linked chitosan/nano-HAp composite framework (GCHF) (c, d), and HAp coated genipin-chitosan conjugation scaffold (HGCCS) (e, f) after 3 days of culture in vitro. Black arrow designates the adherent cells. A much more pronounced protrusion of pseudopodia contacts with network-like HAp nanostructures on the channel surface of HGCCS (f) as indicated by the white frame in (e).

well-known, cell shape is a potent regulator of cell growth and physiology, and many events related to embryonic development and stem cell differentiation are influenced by cell shape.[48] Whether the surface HAp network nanostructure of HGCCS can affect the differentiation of rat BMSCs needs to be investigated in the future work.

3.6. Cell Proliferation. As shown in Figure 8, the result of a cell proliferation assay clearly demonstrates that rat BMSCs on GCF, GCHF and HGCCS exhibit a good growth state, even when the culturing period is extended, which indicates that these three kinds of biomaterials have good biocompatibility for rat

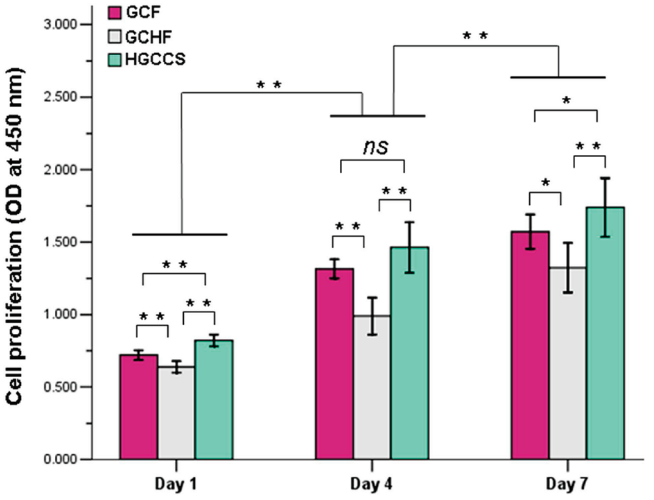

Figure 8. Proliferation of rat BMSCs on genipin-cross-linked chitosan framework (GCF), chitosan/nano-HAp composite framework (GCHF), and HAp-coated genipin-chitosan conjugation scaffold (HGCCS). Data are presented as mean ± standard deviation with $n = 6$ ($^{*}P < 0.05$, $^{**}P < 0.01$).

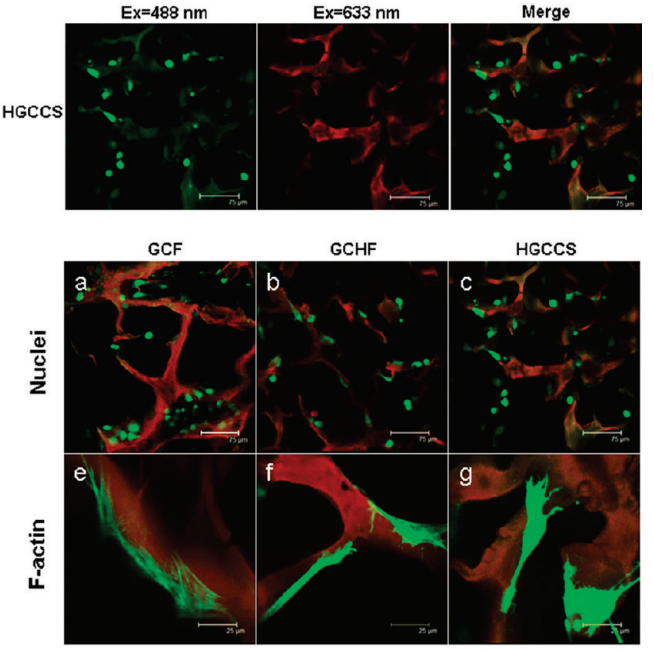

Figure 9. CLSM images of the distribution and the changes in actin cytoskeleton organization of rat BMSCs cultured for 3 days on the genipin-cross-linked chitosan framework (GCF) (a, e), genipin-cross-linked chitosan/nano-HAp composite framework (GCHF) (b, f), and HAp coated genipin-chitosan conjugation scaffold (HGCCS) (c, g) after nuclei and F-actin staining with acridine orange (AO) and Alexa Fluor 488 phalloidin, respectively. The bright green dots and regions are nuclei and cytoskeleton, respectively, and the dark red regions are the scaffolds.

BMSCs. Meanwhile, compared to GCF, rat BMSCs tend to have higher viability on HGCCS, while growing slower on GCHF.

The result reveals that HAp network-like nanostructures mineralized on the channel surface of HGCCS significantly enhances proliferation. The unique surface structure provides an important cue to regulate cell proliferation through mechanotransduction pathways, or triggers specific protein adsorption for easier access to nutrients by BMSCs. It is generally recognized that integrin-mediated cell-matrix interaction regulates cellular survival in multiple ways. With respect to GCHF, the irregular surface geometry due to the nonuniform distribution of HAp nanorods may not promote cell adhesion and growth,[49] which confirms the SEM observations (Figure 7).

In addition, it is worth mentioning that although GCF, GCHF and HGCCS display different proliferation states, it should be emphasized that the higher level of rat BMSCs proliferation on HGCCS, relative to GCF and GCHF, might not be due purely to surface characteristics, although differences in scaffold seeding efficiency may be ruled out. Importantly, rat BMSCs indeed display the highest proliferation on HGCCS, which confirms a potential advantage for bone tissue engineering.

3.7. Cell Localization and Cytoskeleton Organization. The CLSM images of the distribution and cytoskeleton organization of rat BMSCs cultured on the various chitosan-based scaffolds are shown in Figure 9. The displayed images are obtained by merging two images: one is the fluorescence image of the nuclei or F-actin of rat BMSCs at an excitation wavelength of 488 nm, and the other is the fluorescence image of the 3D scaffold at an excitation wavelength 633 nm (HGCCS as a representative seen in Figure 9). In Figure 9a–c, the bright green dots representing the nuclei clearly display a uniform, extensive and compact distribution of rat BMSCs on GCF, GCHF and HGCCS, respectively. However, corresponding to the result of cell proliferation, GCF and GCHF present higher cells density than GCH. In addition, the fluorescence images (Figure 9 and Figure S3 in the Supporting Information) indicates that GCF, GCHF and HGCCS all possess intrinsic fluorescence, which may provide an effective way to image the cell–scaffold interaction and effectively monitor the adhesion, localization and migration of cells on the surface of the scaffolds.

To examine the direct interaction between cells and the scaffold surface structure, the cytoskeleton organization changes in rat BMSCs (the bright regions) on the channel surface of the biomaterials are displayed in Figure 9e–g. Similar to the results obtained with SEM, rat BMSCs on GCF retain the typical phenotype of BMSCs, and actin stress fibers are seen throughout the cells (Figure 9e). Rat BMSCs on the channel surface of GCHF (Figure 9f) are much thicker than those on the chitosan framework, and are significantly elongated. The cytoskeleton organization (Figure 9g) of rat BMSCs on two-level, three-dimesional networked HGCCS is totally different from that on the chitosan framework (GCF). In addition to the broad area, the rat BMSCs on networked HAp nanostructures produce more protrusions, which presents a more positive response to integrin-mediated cytoskeletal reorganization and cellular adhesion.

It is becoming clear that synthetically nanofabricated topography can influence cell morphology, adhesion, migration and proliferation through intergrin-mediated cytoskeletal tension and modulation of the intracellular signaling pathways that regulate transcriptional level and gene expression.[50] In this study BMSCs directly contacted the substrate and no chemical media were added. Moreover, the integrin-mediated cell-matrix interaction is crucial for outside-in signal transduction. Therefore, we have reason to believe that the change in cytoskeleton organization can be attributed to direct cell mechanotransduction induced by networklike nanostructures on the channel wall, thereby causing cellular gene expression profiles and functions of rat BMSCs.[36,51,52] Our future work will focus on the effects of

the HGCCS surface characteristics on the osteoblastic commitment of BMSCs

4. CONCLUSIONS

In summary, our studies have demonstrated the construction of a 2-level 3D networked HAp coated genipin-chitosan conjugation scaffold by assembling HAp nanostructures on the chitosan framework through induced nanocrystallon biomimetic mineralization in SBF. The first level is the chitosan framework with interconnected channels, and the second level is the nanonetwork and nanostructure of HAp formed on the channel surface of the chitosan framework. Nontoxic genipin is used as a cross-linker and it endows high strength and intrinsic fluorescence to the chitosan framework. Rod-like HAp nanocrystals and the HAp nanonetwork found on the channel surface reinforce the scaffold that is produced. The intrinsic fluorescence facilitates cellular imaging and biodegradation studies. Furthermore, by culturing rat BMSCs on HGCCS in vitro, we have demonstrated its high biocompatibility. We have observed the influence of biomimetically mineralized HAp nanostructures on cellular morphology and cytoskeleton organization of rat BMSCs. The observed change in cellular morphology and integrin-mediated cytoskeletal tension can be attributed to the HAp nanonetwork and nanostructures. Our research provides a novel research avenue to construct a scaffold for bone tissue engineering, monitor scaffold biodegradation with intrinsic fluorescence, and investigate the impact of the nanostructures and material surfaces on stem cell functions.

■ ASSOCIATED CONTENT

Ⓢ Supporting Information. Figures showing TEM observation and XRD analysis of nano-HAp powders, FTIR analysis of scaffolds, and fluorescence images of GCHF and HGCCS seeded BMSCs. This material is available free of charge via the Internet at http://pubs.acs.org.

■ AUTHOR INFORMATION

Corresponding Author
*E-mail: hongliu@sdu.edu.cn. Tel.: (+86) 531-88362807. Fax: (+86) 531-88574135.

■ ACKNOWLEDGMENT

This research was supported by an NSFC (NSFDYS: 50925205, 50872070, Grant 50990303, Innovation Research Group, 50721002), Independent Innovation Foundation of Shandong University (IIFSDU, 2009JC011), and Graduate Independent Innovation Foundation of Shandong University (GIIFSDU, yzc09064). Authors would like to give their heartfelt thanks to Prof. Si-Shen Feng (National University of Singapore) for his guidance and discussion, and Prof. Robert I. Boughton (Chair, Department of Physics and Astronomy, Bowling Green State University, USA) for his thorough revision.

■ REFERENCES

(1) Hall, M. J.; Owings, M. F. *Adv. Data* **2002**, *329*, 1–18.
(2) Rose, F. R.; Oreffo, R. O. *Biochem. Biophys. Commun.* **2002**, *292*, 1–7.
(3) Linkhart, T. A.; Mohan, S.; Baylink, D. J. *Bone* **1996**, *19*, 1S–12S.
(4) Rezwan, K.; Chen, Q. Z.; Blaker, J. J.; Boccaccini, A. R. *Biomaterials* **2006**, *27*, 3413–3431.
(5) Hollister, S. J. *Nat. Mater.* **2005**, *4*, 518–524.
(6) Johnson, P. C.; Mikos, A. G.; Fisher, J. P.; Jansen, J. A. *Tissue Eng.* **2007**, *13*, 2827–2837.
(7) Martin, C.; Winet, H.; Bao, J. Y. *Biomaterials* **1996**, *17*, 2373–2380.
(8) Burg, K. J.; Porter, S.; Kellam, J. F. *Biomaterials* **2000**, *21*, 2347–2359.
(9) Zhang, W.; Liao, S. S.; Cui, F. Z. *Chem. Mater.* **2003**, *15*, 3221–3226.
(10) Kim, I. Y.; Seo, S. J.; Moon, H. S.; Yoo, M. K.; Park, I. Y.; Kim, B. C.; Cho, C. S. *Biotechnol. Adv.* **2008**, *26*, 1–21.
(11) Kumar, M. N.; Muzzarelli, R. A.; Muzzarelli, C.; Sashiwa, H.; Domb, A. J. *Chem. Rev.* **2004**, *104*, 6017–6084.
(12) Thein-Han, W. W.; Misra, R. D. *Acta Biomater.* **2009**, *5*, 1182–1197.
(13) Zhao, F.; Grayson, W. L.; Ma, T.; Bunnell, B.; Lu, W. W.; *Biomaterials* **2006**, *27*, 1859–1867.
(14) Hu, Q. L.; Li, B. Q.; Wang, M.; Shen, J. *Biomaterials* **2004**, *25*, 779–785.
(15) Manjubala, I.; Scheler, S.; Bossert, J.; Jandt, K. D. *Acta Biomater.* **2006**, *2*, 75–84.
(16) Bigi, A.; Cojazzi, G.; Panzavolta, S.; Rubini, K.; Roveri, N. *Biomaterials* **2001**, *22*, 763–768.
(17) Ohtsuki, C.; Kamitakahara, M.; Miyazaki, T. *J Tissue Eng. Regen. Med.* **2007**, *1*, 33–38.
(18) Zhang, W.; Liao, S. S.; Cui, F. Z. *Chem. Mater.* **2003**, *15*, 3221–3226.
(19) Li, X.; Xie, J.; Lipner, J; Yuan, X.; Thomopoulos, S.; Xia, Y. *Nano Lett* **2009**, *9*, 2765–2768.
(20) Malafaya, P. B.; Reis, R. L. *Acta Biomater* **2009**, *5*, 644–660.
(21) Kong, L.; Gao, Y.; Lu, G.; Gong, Y.; Zhao, N.; Zhang, X. *Eur. Polym. J.* **2006**, *42*, 3171–3179.
(22) Zhang, L.; Li, Y. B.; Yang, A. P.; Peng, X. L.; Wang, X. J.; Zhang, X. *J. Mater. Sci. Mater. Med.* **2005**, *16*, 213–219.
(23) Araújo, A. B.; Lemos, A. F.; Ferreira, J. M. *J. Biomed. Mater. Res., A* **2009**, *88*, 916–922.
(24) Chen, S. C.; Wu, Y. C.; Mi, F. L.; Lin, Y. H.; Yu, L. C.; Sung, H. W. *J. Controlled Release* **2004**, *96*, 285–300.
(25) Chen, H.; Ouyang, W.; Lawuyi, B.; Martoni, C.; Prakash, S. *J, Biomed, Mater, Res A* **2005**, *75*, 917–927.
(26) Chen, H.; Ouyang, W.; Lawuyi, B.; Prakash, S. *Biomacromolecules* **2006**, *7*, 2091–2098.
(27) Kuo, Y. C.; Lin, C. Y. *Biotechnol. Bioeng.* **2006**, *95*, 132–144.
(28) Kuo, Y. C.; Yeh, C. F.; Yang, J. T. *Biomaterial* **2009**, *30*, 6604–6613.
(29) Kokubo, T.; Takadama, H. *Biomaterials* **2006**, *27*, 2907–2915.
(30) O'Brien, F. J.; Harley, B. A.; Yannas, I. V.; Gibson, L. J. *Biomaterials* **2005**, *26*, 433–441.
(31) Ohgushi, H.; Kotobuki, N.; Funaoka, H.; Machida, H.; Hirose, M.; Tanaka, Y.; Takakura, Y. *Biomaterials* **2005**, *26*, 4654–4661.
(32) Rahaman, M. N.; Mao, J. J. *Biotechnol. Bioeng.* **2005**, *91*, 261–284.
(33) Qi, S.; Yi, C.; Ji, S.; Fong, C. C.; Yang, M. *ACS Appl, Mater, Interfaces* **2009**, *1*, 30–34.
(34) Jiang, K.; Fan, D.; Belabassi, Y.; Akkaraju, G.; Montchamp, J. L.; Coffer, J. L. *ACS Appl Mater Interfaces* **2009**, *1*, 266–269.
(35) Bettinger, C. J.; Langer, R.; Borenstein, J. T. *Angew. Chem., Int. Ed.* **2009**, *48*, 5406–5415.
(36) Stevens, M. M.; George, J. H. *Science* **2005**, *310*, 1135–1138.
(37) Dalby, M. J.; Gadegaard, N.; Tare, R.; Andar, A.; Riehle, M. O.; Herzyk, P.; Wilkinson, C. D.; Oreffo, R. O. *Nat. Mater.* **2007**, *6*, 997–1003.
(38) Neira1, I. S.; Guitián, F.; Taniguchi1, T.; Watananbe, T.; Yoshimura, M. *Mater. Sci.* **2008**, *43*, 2171–2178.
(39) Olszta, M. J.; Cheng, X. G.; Jee, S. S.; Kumar, R.; Kim, Y. Y.; Kaufman, M. J.; Douglas, E. P.; Gower, L. B. *Mater. Sci. Eng., R* **2007**, *58*, 77–116.
(40) Nukavarapu, S. P.; Kumbar, S. G.; Brown, J. L.; Krogman, N. R.; Weikel, A. L.; Hindenlang, M. D.; Nair, N. S.; Allcock, H. R.; Laurencin, C. T. *Biomacromolecules* **2008**, *9*, 1818–1825.

(41) Lee, K. W.; Wang, S.; Yaszemski, M. J.; Lu, L. *Biomaterials* **2008**, *29*, 2839–2848.
(42) Takahashi, Y.; Yamamoto, M.; Tabata, Y. *Biomaterials* **2005**, *26*, 3587–3596.
(43) Pittenger, M. F.; Mackay, A. M.; Beck, S. C.; Jaiswal, R. K.; Douglas, R.; Mosca, J. D.; Moorman, M. A.; Simonetti, D. W.; Craig, S.; Marshak, D. R. *Science* **1999**, *284*, 143–147.
(44) Wang, N.; Xie, K.; Huo, S. W.; Zhao, J.; Zhang, S.; Miao, J. *J. Cell Biochem.* **2007**, *100*, 1548–1557.
(45) Oliveira, J. M.; Rodrigues, M. T.; Silva, S. S.; Malafaya, P. B.; Gomes, M. E.; Viegas, C. A.; Dias, I. R.; Azeverdo, J. T.; Mano, J. F.; Reis, R. L. *Biomaterials* **2006**, *27*, 6123–6137.
(46) Becher, P. F. *J. Am. Ceram. Soc.* **1991**, *74*, 255–269.
(47) Brammer, K. S.; Oh, S.; Gallagher, J. O.; Jin, S. *Nano Lett.* **2008**, *8*, 786–793.
(48) Guilak, F.; Cohen, D. M.; Estes, B. T.; Gimble, J. M.; Liedtke, W.; Chen, C. S. *Cell Stem Cell* **2009**, *5*, 17–26.
(49) Chen, C. S.; Mrksich, M.; Huang, S.; Whitesides, G. M.; Ingber, D. E. *Science* **1997**, *276*, 1425–1428.
(50) McBeath, R.; Pirone, D. M.; Nelson, C. M.; Bhadriraju, K.; Chen, C. S. *Dev. Cell* **2004**, *6*, 483–495.
(51) Vogel, V.; Sheetz, M. *Nat. Rev. Mol. Cell Biol.* **2006**, *7*, 265–275.
(52) Geiger, B.; Spatz, J. P.; Bershadsky, A. D. *Nat. Rev. Mol. Cell Biol.* **2009**, *10*, 21–33.